Research Square

Preprints are preliminary reports that have not undergone peer review.
They should not be considered conclusive, used to inform clinical practice,
or referenced by the media as validated information.

Trace Nickel Doping Tailors Grain-Boundary Energetics for Low-Temperature Cu–Cu Bonding

Chih Chen

chihchen@nycu.edu.tw

National Yang Ming Chiao Tung University

Hsin-Lin Kai

National Yang Ming Chiao Tung University

Ming-Han Lu

National Chung Hsing University

Chen-Ning Li

National Yang Ming Chiao Tung University

Chih-Chi Tsai

National Yang Ming Chiao Tung University

Yi-Chen Chung

National Yang Ming Chiao Tung University

Ke-Wei Hsieh

National Yang Ming Chiao Tung University

Article

Keywords:

Posted Date: November 13th, 2026

DOI: https://doi.org/10.21203/rs.3.rs-11337729/v1

License: This work is licensed under a Creative Commons Attribution 4.0 International License.
Read Full License

Additional Declarations: There is **NO** Competing Interest.

Trace Nickel Doping Tailors Grain-Boundary Energetics for Low-Temperature Cu–Cu Bonding

Abstract

In this study, trace Ni-doped nanocrystalline Cu films were prepared via co-electroplating to investigate the relationship between varying trace Ni concentrations, grain-boundary energetics, and low-temperature bondability. Experimental results indicated that trace nickel doping tailors the grain boundary energetics of nanocrystalline Cu, highlighting a relationship between thermodynamic stability and low-temperature bondability. While Cu-0.25Ni$_{(171\ nm)}$ exhibits enhanced thermal stability via twin-boundary relaxation, the finer-grained Cu-0.5Ni$_{(124\ nm)}$ stores considerable grain-boundary energy, rendering it thermodynamically active. Interestingly, this energetic state provides a potent driving force during thermocompression at 250 °C; the release of stored energy helps overcome diffusion barriers, triggering significant cross-interface grain growth and yielding a robust shear strength of 120 MPa. Harnessing this mechanism, we design an asymmetric bonding architecture pairing the stable Cu-0.25Ni$_{(171\ nm)}$ with the active Cu-0.5Ni$_{(124\ nm)}$. This interfacial thermal stability gradient promotes pronounced unidirectional grain boundary migration, effectively eliminating the original interface to achieve a high shear strength of 153 MPa. This grain boundary engineering strategy offers a promising pathway to balance structural stability and bondability, providing a practical thermodynamic framework for next-generation advanced packaging.

Introduction

For decades, the semiconductor industry has relied on two-dimensional (2D)

planar scaling to drive device performance and increase transistor density. However, as transistor nodes approach their fundamental physical limits, traditional 2D scaling is increasingly bottlenecked by severe interconnect RC delays, power dissipation, and escalating manufacturing costs [1, 2]. To bypass these physical limitations and extend Moore's law, three-dimensional integrated circuits (3D ICs) have emerged as a highly promising solution. By shifting from planar integration to vertical chip stacking, 3D ICs significantly reduce interconnection lengths and enable ultra-high integration density, making vertical stacking essential for advanced packaging [3, 4]. Current vertical interconnects mainly rely on copper joints capped with solder. However, as packaging pitches decrease, solder is prone to extrusion during bonding, leading to electrical shorts, while the necessary reduction in solder volume inherently exacerbates void formation [5, 6]. Reducing solder amounts at finer pitches introduces other reliability issues [7-9]. Therefore, direct copper-to-copper (Cu-Cu) bonding is gaining attention as an alternative to provide higher interconnect density for pitches of 10 μm and below.

Widely recognized as the optimal candidate to replace traditional microbumps, Cu offers intrinsic advantages, including exceptional electrical and thermal conductivities and outstanding electromigration resistance [10, 11]. By establishing a direct metallurgical bond, this technology eliminates the reliability hazards associated with solder joints while effectively mitigating parasitic capacitance and resistance (RC delay) within the interconnect architecture. As a result, direct Cu-Cu bonding can achieve I/O density to the 100-million level, representing a substantial increase of two to three orders of magnitude over conventional microbump technologies [12-14].

Currently, thermo-compression is a common method for direct Cu-Cu bonding.

To achieve a complete bond, this process usually requires temperatures above 300 °C to drive atomic diffusion. However, high temperatures can damage temperature-sensitive components and cause issues such as thermal stress and wafer warpage [15]. Thus, developing reliable Cu-Cu bonding below 300 °C is an important goal for industrial applications.

At lower temperatures, the atomic diffusion rate decreases, making interfacial bonding more difficult. Many studies use external surface modifications to solve this issue. For example, surface-activated bonding effectively removes surface oxides and enables bonding at room temperature; however, it requires an ultra-high vacuum, thereby increasing manufacturing costs [16-18]. Other methods, such as noble metal passivation or plasma treatments, are time-consuming and rely heavily on external treatments, which often lead to complicated processes or residue-related strength degradation [19-22].

To address these limitations, this study explores microstructural engineering of the Cu film by employing nanocrystalline copper (NC-Cu). The high density of grain boundaries in NC-Cu provides abundant fast-diffusion pathways, thereby facilitating sufficient atomic diffusion at low temperatures [23-25]. It also exhibits thermal expansion properties that assist with interfacial contact [26, 27]. However, NC-Cu is prone to self-annealing even at room temperature, leading to time-dependent microstructural evolution that compromises storage stability and narrows the process window [28-30].

To mitigate the self-annealing of NC-Cu while preserving its low-temperature bonding capability, trace amounts of nickel (Ni) are added to the Cu film during

electroplating. Incorporating Ni is intended to suppress grain growth and stabilize the nanocrystalline microstructure during storage. By tailoring the microstructure through controlled Ni incorporation, the low-temperature bonding strength and interfacial integrity can be further enhanced.

Results

· Characterization of NC-Cu-Ni Films

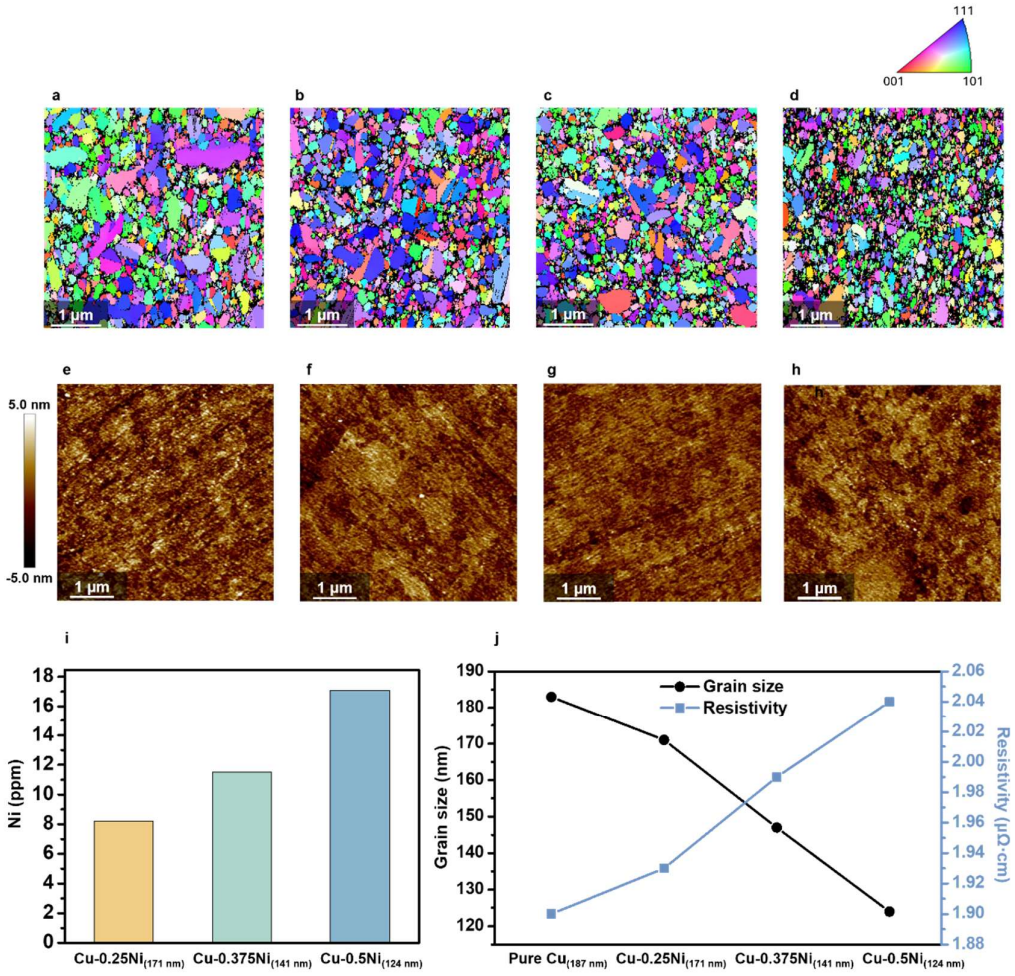
To systematically evaluate the effect of Ni concentration on microstructural evolution, the electrodeposited thin films were characterized using electron backscatter diffraction (EBSD) and orientation imaging microscopy (OIM). Based on the Ni content in the electrolyte and the corresponding average grain sizes, the samples are denoted as Pure $Cu_{(187\ nm)}$, Cu-0.25$Ni_{(171\ nm)}$, Cu-0.375$Ni_{(141\ nm)}$, and Cu-0.5$Ni_{(124\ nm)}$. As shown in Fig. 1a-d, the Pure Cu film exhibited an average grain size of approximately 187 nm. Adding Ni to the co-electroplating bath showed a clear and systematic grain-refinement trend. The average grain sizes decreased to 171 nm, 141 nm, and 124 nm for the Cu-0.25Ni $_{(171\ nm)}$, Cu-0.375$Ni_{(141\ nm)}$, and Cu-0.5Ni $_{(124\ nm)}$, respectively. This pronounced grain refinement is primarily attributed to the incorporated trace Ni atoms, which provide abundant nucleation sites during co-electrodeposition. These sites effectively promote the nucleation rate, thereby suppressing subsequent grain growth.

Furthermore, to ensure the interfacial conformability required for subsequent low-temperature bonding, the post-CMP surface topography of all samples was characterized using atomic force microscopy (AFM). The AFM analysis (Fig. 1e-h) confirmed exceptionally clean surfaces devoid of residual slurry. Notably, the root-mean-square (Rq) roughness of all sample groups was consistently maintained between 1.0 and 1.3 nm, showing no significant variation with increasing Ni concentration. This ultra-smooth topography shows the stringent requirement ($Rq < 2$ nm) for achieving high-quality direct Cu-Cu bonding[31]. Consequently, this eliminates surface roughness disparities as a confounding variable affecting the

overall results in subsequent bonding experiments.

To evaluate electrical performance and quantify internal film composition, the samples were further characterized using a four-point probe system and inductively coupled plasma mass spectrometry (ICP-MS). As shown in Fig. 1i, quantitative analysis revealed that the actual Ni content incorporated into the films scaled proportionally with the electrolyte concentration but remained exceptionally low (< 20 ppm). As depicted in Fig. 1j, along with the systematic grain refinement, the absolute resistivity exhibited a predictable upward trend with grain size of the films, rising from 1.97 μΩ·cm (87.5% IACS) for the pure Cu film to 2.10 μΩ·cm (82.1% IACS) for the highest doped sample. This slight increase in resistivity is primarily driven by the intrinsically higher resistivity of trace Ni atoms and the increased volume fraction of grain boundaries, which intensifies electron scattering.

Fig. 1: Characterization of the electrodeposited NC-Cu-Ni Films.



EBSD maps of as-fabricated samples: (**a**) Pure $Cu_{(187\ nm)}$, (**b**) Cu-0.25$Ni_{(171\ nm)}$, (**c**) Cu-0.375$Ni_{(141\ nm)}$, (**d**) Cu-0.5$Ni_{(124\ nm)}$. AFM surface topographies of the corresponding samples after CMP and surface cleaning: (**e**) Pure $Cu_{(187\ nm)}$, (**f**) Cu-0.25$Ni_{(171\ nm)}$, (**g**) Cu-0.375$Ni_{(141\ nm)}$, (**h**) Cu-0.5$Ni_{(124\ nm)}$. **i** Ni content incorporated in different films. j Correlation between the average grain size and electrical resistivity of the deposited films.

- **Self- annealing and thermal stability of NC-Cu-Ni Films**

To evaluate the microstructural evolution under thermal conditions relevant to the bonding processes, the thin films were annealed at elevated temperatures. The resulting grain sizes and normalized grain growth ratios ($\Delta g/g_0$) are presented in Fig. 2a, b. The results show that grain growth was progressively accelerated with increasing annealing temperature. At a low annealing temperature of 150 °C, the normalized $\Delta g/g_0$ remained modest between 0.5 and 1.5. Increasing the temperature to 200 °C led to a slight rise in the growth ratio. Crucially, at 250 °C—a critical temperature mimicking the actual bonding condition—significant grain coarsening occurred, with the growth ratio notably increasing to 2–6 fold. Upon further heating to 280 °C, however, grain coarsening accelerated markedly, increasing the grain size to 5–8 fold.

Notably, the Cu-0.5Ni$_{(124\ nm)}$ film shows the most drastic microstructural transformation among all conditions. Starting from an initial grain size of ~124 nm, its average grain size expanded dramatically to ~900 nm at 250 °C and ultimately to ~1 μm after annealing at 280 °C, an 8-fold increase. This pronounced growth behavior is intrinsically linked to its initial state: the extremely fine initial grains store substantial grain boundary excess energy and provide rapid pathways for atomic diffusion. Upon thermal activation at 250 and 280 °C, rapid release of the stored energy provides a strong driving force for grain-boundary migration, promoting the growth of larger grains at the expense of neighboring fine grains and thereby reducing the overall grain-boundary energy.

Previous studies have demonstrated that pure NC-Cu is highly susceptible to

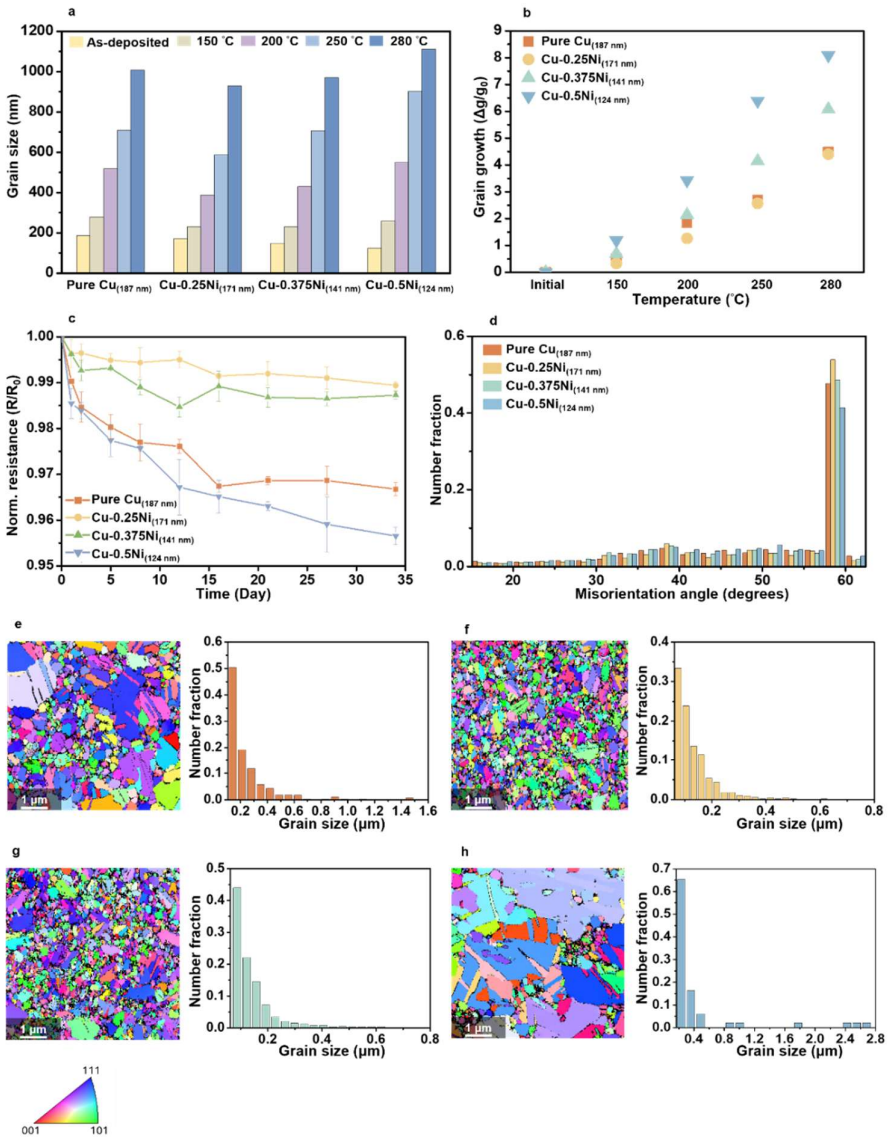
spontaneous self-annealing, even at room temperature. This study systematically investigates the room-temperature self-annealing behavior of electrodeposited NC-Cu-Ni films over 30 days of storage. As depicted in Fig. 2c, the magnitude of the normalized resistivity drop (R/R_0) followed an ascending order of Cu-0.25Ni$_{(171\ nm)}$ < Cu-0.375Ni$_{(141\ nm)}$ < Pure Cu$_{(187\ nm)}$ < Cu-0.5Ni$_{(124\ nm)}$. Notably, the Cu-0.25Ni$_{(171\ nm)}$ film showed remarkable resistivity stability, with a reduction of less than 1%. Consistent with these macroscopic electrical measurements, EBSD analysis after 30 days (Fig. 2e-h) revealed highly correlated microstructural evolution. While the Pure Cu$_{(187\ nm)}$ and Cu-0.5Ni$_{(124\ nm)}$ films experienced partial and substantial grain growth, respectively, the grain size of the Cu-0.25Ni$_{(171\ nm)}$ film remained remarkably unchanged. This exceptional room-temperature thermal stability effectively suppresses self-annealing, thereby significantly extending the allowable queue time in industrial semiconductor manufacturing processes.

To elucidate the physical mechanism behind the superior stability of the Cu-0.25Ni$_{(171\ nm)}$ film, we analyzed grain-boundary misorientation angles using OIM.

As shown in Fig. 2d, the Cu-0.25Ni$_{(171\ nm)}$ film exhibited a pronounced peak near 60°, indicating a high volume fraction of twin boundaries. Previous studies have shown that coherent Σ3 twin boundaries possess ultra-low excess interfacial energy compared to random high-angle grain boundaries[32, 33]. Consequently, this high density of twin structures minimizes total free energy, making the Cu-0.25Ni$_{(171\ nm)}$ film thermodynamically stable and highly resistant to self-annealing. Conversely, the Cu-0.5Ni$_{(124\ nm)}$ film showed severe self-annealing, with microstructural degradation even surpassing that of Pure Cu$_{(187\ nm)}$. This instability reduced its ultra-fine initial grain size, which inherently introduces an exceptionally high density of grain

boundaries**.** Consequently, the system resides in a thermodynamically unstable state with excessive stored grain-boundary energy. During room-temperature storage, the system spontaneously releases this stored free energy, driving grain coarsening.

Fig. 2: Self- annealing and thermal stability of NC-Cu-Ni Films



a Average grain size evolution of the different films after annealing at various temperatures. **b** Grain growth behavior of the distinct films as a function of annealing temperature. **c** Electrical resistance drop of the corresponding films during room-temperature storage. **d** Misorientation angle distributions of the respective films. EBSD maps of the films after 30 days of room-temperature storage, demonstrating their microstructural stability: (**e**) Pure $Cu_{(187\ nm)}$, (**f**) $Cu\text{-}0.25Ni_{(171\ nm)}$, (**g**) $Cu\text{-}0.375Ni_{(141\ nm)}$, (**h**) $Cu\text{-}0.5Ni_{(124\ nm)}$.

- **Cu–Cu direct bonding using NC-Cu-Ni Films**

To evaluate the bonding quality of the NC-Cu-Ni films, the interfacial microstructure of the bonded dies was systematically characterized. From Fig. 3a-d, all NC-Cu-Ni samples achieved intimate contact with minimal interfacial voids under a bonding pressure of 22 MPa at 200 °C. All samples demonstrated that the original bonding interfaces remained distinct and flat**.** The highly stable Cu-0.25Ni$_{(171\ nm)}$ and Cu-0.375Ni$_{(141\ nm)}$ retained fine nanograins, whereas pure Cu$_{(187\ nm)}$ and Cu-0.5Ni$_{(124\ nm)}$ exhibited considerable grain coarsening. The limited thermal budget at 200 °C was insufficient to overcome the energy barrier for cross-interface grain-boundary migration.

Increasing the bonding temperature to 250 °C for 1 hour resulted in distinct interfacial evolution. As shown in Fig. 3e-h, the Cu-0.5Ni$_{(124\ nm)}$ variant sustained robust cross-interface grain growth, achieving a high interfacial zig-zag ratio of ~1.1 (defined as the actual contour length divided by the projected flat length). This exceptional low-temperature bonding capability was intrinsically governed by its ultra-fine initial grain size. The extremely high grain-boundary density provided rapid atomic diffusion pathways. This effect triggered spontaneous grain coarsening that heavily consumed the original interface, resulting in a zig-zag interfacial morphology that ensured superior bonding integrity.

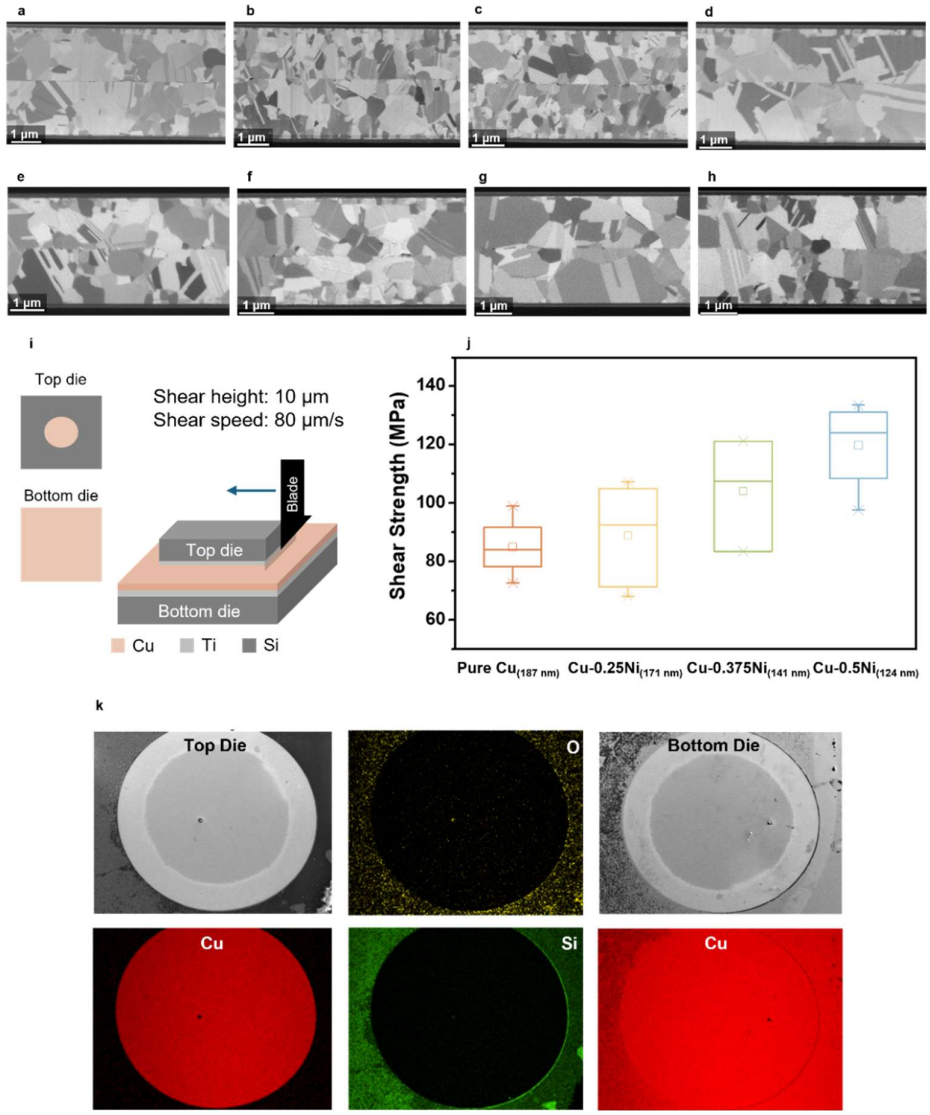
Furthermore, the Cu-0.375Ni$_{(141\ nm)}$ variant presented a compelling strategic alternative. While its cross-interface grain growth was slightly less aggressive than that of Cu-0.5Ni$_{(124\ nm)}$, it showed significantly superior thermal stability against self-annealing, as established in the previous section. By comprehensively balancing

the allowable queue time for industrial manufacturing and the bonding capability, Cu-0.375Ni$_{(141\ nm)}$ emerged as the optimal engineered solution.

To evaluate the mechanical strength of samples bonded at 250 °C, shear testing was conducted. To obtain a reliable evaluation of joint strength, we pre-patterned the top Cu dies into micro-mesa structures to reduce the effective contact area, as schematically illustrated in Fig. 3i. As shown in Fig. 3j, the measured shear strength aligns well with the interfacial microstructures observed earlier. Shear strength increases with Ni concentration, reaching ~120 MPa for the Cu-0.5Ni$_{(124\ nm)}$ sample, despite the reduced bonding area.

To further understand interface failure behavior, the fracture surfaces were examined using EDS analysis, as shown in Fig. 3k. The elemental results show a dominant Cu signal across the ruptured area, with no clear detection of substrate elements. This indicates that the fracture occurred mainly within the Cu layer and along the Cu-Cu interface rather than at the substrate boundary. These observations suggest that the pre-patterned design helps concentrate the stress at the joint, allowing the shear testing data to reflect the bonding quality of the Cu-Cu interface more effectively.

Fig. 3: Cu–Cu direct bonding using NC-Cu-Ni Films.



Cross-sectional images of the joints bonded at 200 °C for 1 h: (**a**) Pure $Cu_{(187\ nm)}$, (**b**) Cu-0.25$Ni_{(171\ nm)}$, (**c**) Cu-0.375$Ni_{(141\ nm)}$, (**d**) Cu-0.5$Ni_{(124\ nm)}$. Cross-sectional images of the joints bonded at 250 ˚C for 1h: (**e**) Pure $Cu_{(187\ nm)}$, (**f**) Cu-0.25$Ni_{(171\ nm)}$, (**g**) Cu-0.375$Ni_{(141\ nm)}$, (**h**) Cu-0.5$Ni_{(124\ nm)}$. **i** Schematic illustration of the die shear test setup alongside the as-prepared test samples. **j** Shear strength results for all bonded configurations. **k** EDS elemental mapping across the bonding interface, revealing a predominant Cu signal that confirms cohesive failure exclusively within

- **Cu–Cu direct bonding using different thermal stabilities**

Previous analyses of the fundamental properties and thermal stabilities of the various films revealed that altering the Ni doping concentration creates significant differences in the microstructural and thermodynamic states of the materials. The literature suggests that Cu films with different initial grain sizes or internal stress states for asymmetric bonding often show superior bonding quality compared to homogeneous films[34]**.** Building upon this theoretical foundation, this study proposes a bonding strategy based on a thermal stability gradient. Specifically, the highly thermally stable Cu-0.25Ni$_{(171\ nm)}$ film and the highly unstable Cu-0.5Ni$_{(124\ nm)}$ film were selected for asymmetric bonding to investigate microstructural bonding behavior using a cross-interface energy gradient.

As shown by the cross-sectional analysis in Fig. 4a, under a thermocompression condition of 200 °C, the bonding interface of this asymmetric system—comprising the thermally stable Cu-0.25Ni$_{(171\ nm)}$ layer on top and the unstable Cu-0.5Ni$_{(124\ nm)}$ layer at the bottom—exhibited significant cross-interface grain growth**.** In contrast, previous symmetric bonding systems completely failed to overcome the interfacial energy barrier under the same low thermal budget.

When the bonding temperature was increased to 250 °C (Fig. 4b), cross-interface grain-boundary migration increased markedly, with a substantially higher density of migrating boundaries than that observed in symmetric bonding at the same temperature. We further analyze the bonding samples using EBSD to investigate grain-growth behavior, as shown in Fig 4c, d (200 °C and 250 °C). Further examination of the overall microstructure reveals that the top thermally stable layer

retained its fine nanocrystalline structure, whereas the bottom unstable layer underwent substantial grain coarsening, consistent with the preceding grain-evolution analysis.

Further TEM examination of the sample bonded at 250 °C (Fig. 4e) provided deeper insights into the interfacial evolution. Selected-area electron diffraction (SAD) patterns (Fig. 4f, g) further substantiate the trans-boundary grain growth by revealing consistent crystallographic orientations across the interface. Finally, energy-dispersive X-ray spectroscopy (EDS) line scans (Fig. 4h) confirmed a pristine metallurgical bond, with no detectable oxides or other residual impurities at the interface. Using the sparsely distributed nanovoids as geometric markers of the original interface (Fig. 4f), it is clearly observable that these voids were ultimately encapsulated within the newly grown, coarse cross-interface grains. This microstructural feature not only demonstrates that the grain-boundary migration velocity vastly exceeded the volumetric diffusion rate of the voids, but also provides definitive physical evidence of a unidirectional grain-growth mode, advancing predominantly from the bottom Cu-0.5Ni$_{(124\ nm)}$ layer into the top Cu-0.25Ni$_{(171\ nm)}$ layer.

While cross-sectional TEM confirms trans-interface grain growth, plan-view TEM was further employed to provide a comprehensive two-dimensional assessment of bonding quality by revealing residual nanovoids across the interface. The graphs (Fig. 4j, k) clearly show that the bonding interface exhibits extreme densification, with the total void area occupying a mere ~2% of the field of view. The unbonded regions predominantly manifest as highly localized nanoscale voids below 200 nm; although a limited number of larger voids are present, they are scattered around the grain.

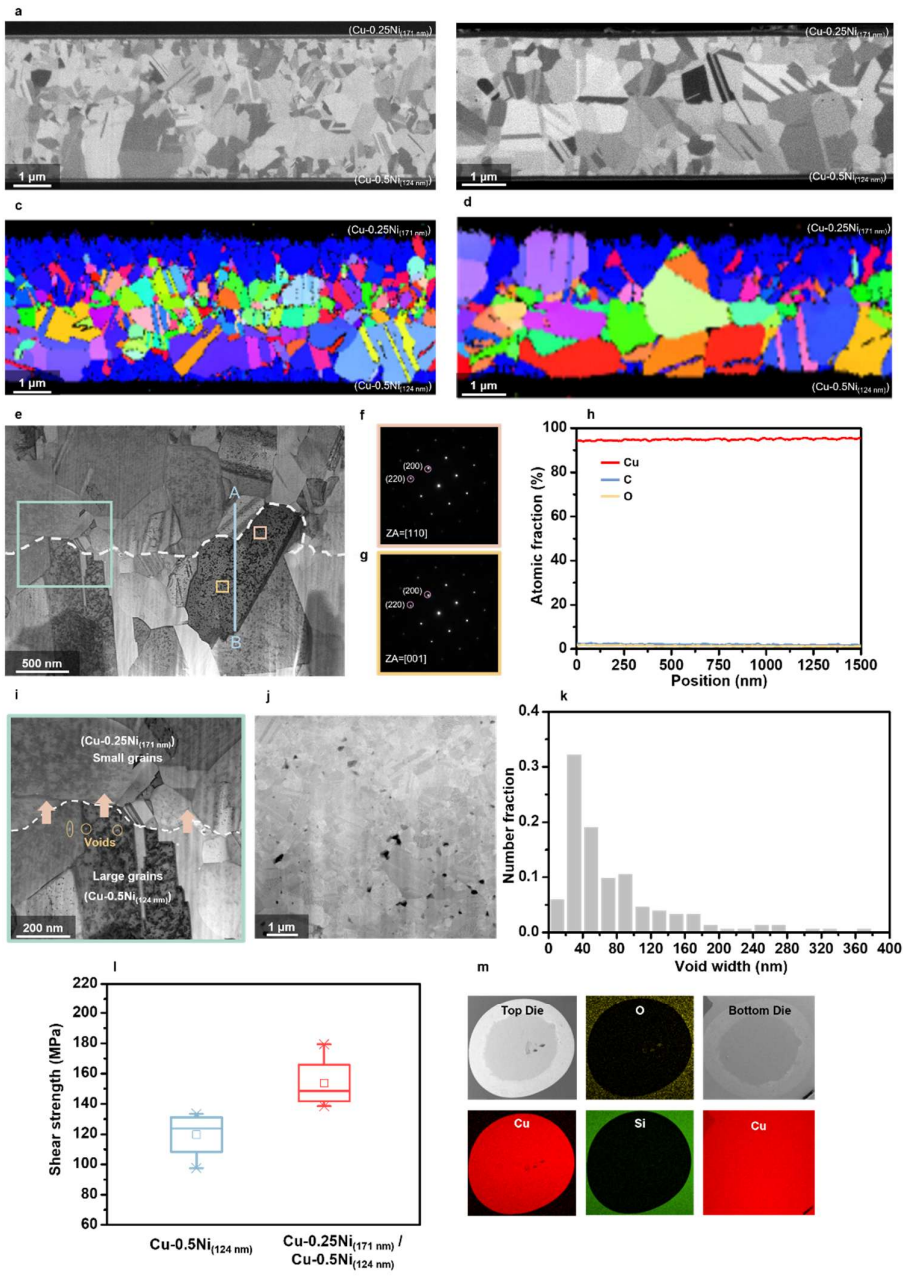
This exceptional low-temperature bonding characteristic stems from the intense thermodynamic driving force induced by the asymmetric thermal stability of the materials on either side of the interface. During the thermal excitation phase, the underlying Cu-0.5Ni$_{(124\ nm)}$ layer first underwent severe grain coarsening, transforming into a coarse-grained network characterized by low grain-boundary density and a low free-energy state. Meanwhile, the top Cu-0.25Ni$_{(171\ nm)}$ layer maintained its nanograins, which were rich in grain boundaries and in a high free-energy state. When these grains with vastly different energy states came into contact, the system generated a powerful driving force to minimize the total free energy, compelling the low-energy coarse grains to consume the adjacent high-energy fine grains. Consequently, the grain boundaries migrated substantially into the upper layer. This cross-interface consumption process driven by the energy gradient eliminated the original flat interface by replacing it with a highly interlocked zig-zag microstructure, thereby delivering outstanding mechanical quality for low-temperature bonding.

To quantitatively evaluate the bonding strength resulting from the thermal stability gradient, we performed die shear testing on asymmetric Cu-0.25Ni / Cu-0.5Ni joints bonded at 250 °C under 22 MPa for 1 hour. As shown in Fig. 4l, the asymmetric bonding configuration exhibited substantially enhanced mechanical performance compared with its symmetric counterparts. Specifically, the shear strength reached ~153 MPa, representing a greater than 20% improvement over the highest shear strength among all symmetric bonding configurations. This superior mechanical strength aligns with the previously observed microstructural evolution,

confirming that energy-gradient-driven cross-interface grain growth and the resulting tortuous interlocked interface effectively reinforce the joint integrity.

Furthermore, fractographic characterization as shown in Fig. 4m was conducted to elucidate the failure behavior. Elemental analysis via EDS confirmed that the fracture surface was predominantly dominated by Cu signals, with no clear detection of elements from the underlying Ti adhesion layer or Si substrate. This cohesive failure mode within the Cu layer indicates that the structural rupture took place along the metallurgical Cu-Cu interface. Consequently, the measured shear strength of 153 MPa reflects the true bonding quality of the asymmetric interface while avoiding premature adhesive delamination at the substrate level.

Fig. 4: Asymmetric Cu–Cu direct bonding using different thermal stabilities.



Cross-sectional micrographs of the asymmetric joints, comprising a highly stable Cu-0.25Ni$_{(171\ nm)}$ upper layer and a highly active Cu-0.5Ni$_{(124\ nm)}$ upper layer and a highly active (**a**) 200 °C for 1 h, (**b**) 250 °C for 1h. Corresponding EBSD maps for the joints bonded at (**c**) 200 °C for 1 h, (**d**) 250 °C for 1h. **e** Low-angle annular dark-field (LAADF) scanning transmission electron microscopy (STEM) image of the asymmetric joint bonded at 250 °C for 1 h, patterns corresponding to the pink (**f**) and yellow (**g**) highlighted regions. **h** EDS line scan profile along the designated blue line. **i** High-magnification view of the green boxed region in **e**, indicating the unidirectional grain growth advancing from the bottom to the top layer. **j** Plan-view HAADF-STEM image capturing the spatial distribution of the interfacial nanovoids. **k** Statistical distribution of the void widths. **l** Shear strength comparison between the symmetric bonding (Cu-0.5Ni$_{(124\ nm)}$) and asymmetric bonding (Cu-0.25Ni$_{(171\ nm)}$ / Cu-0.5Ni$_{(124\ nm)}$). **m** EDS elemental mapping across the asymmetric bonding interface.

Discussion

This study demonstrates a highly effective microstructural engineering strategy for direct Cu-Cu bonding by utilizing trace-Ni-doped nanocrystalline Cu films. By precisely controlling the Ni co-electrodeposition, we achieved significant grain refinement while maintaining excellent surface planarity. Crucially, we demonstrated that trace Ni doping plays a decisive role in governing the thermodynamic stability of the thin films. The Cu-0.25Ni $_{(171\ nm)}$ configuration, rich in coherent twin boundaries, effectively minimized interfacial energy and showed exceptional resistance to room-temperature self-annealing, ensuring a highly extended queue time for practical manufacturing. Conversely, the ultra-fine Cu-0.5Ni$_{(124\ nm)}$ variant exists in a highly unstable thermodynamic state due to its immense stored grain-boundary energy. We successfully leveraged this inherent instability as a powerful thermodynamic driving force during thermocompression. At 250 °C, the spontaneous release of this stored energy overcame the activation barrier for atomic diffusion, triggering aggressive cross-interface grain growth and forming a highly interlocked zig-zag interface with an outstanding shear strength of 120 MPa. Furthermore, we proposed an asymmetric bonding architecture with a highly stable Cu-0.25Ni$_{(171\ nm)}$ layer and a highly active Cu-0.5Ni$_{(124\ nm)}$ layer. This design strategically establishes a cross-interface thermal stability gradient. Driven by the imperative to minimize total free energy, the unstable Cu-0.5Ni$_{(124\ nm)}$ grains rapidly coarsened and actively migrated across the interface to consume the high-energy fine grains of the Cu-0.25Ni$_{(171\ nm)}$ layer. This energy-gradient-driven mechanism successfully facilitated robust, unidirectional cross-interface bonding at exceptionally low thermal budgets (200 °C and 250 °C), yielding a superior shear strength of 153 MPa that significantly outperforms

symmetric joints. This work not only provides profound insights into the defect-driven thermodynamics of nanocrystalline alloys but also establishes a viable, low-thermal-budget interconnect technology critical for next-generation 3D ICs and high-density advanced packaging.

Methods

- **Sample Preparation and Electroplating**

The substrates were pre-coated with a 100 nm Ti adhesion layer and a 200 nm Cu seed layer via physical vapor deposition, into 2.5 × 3.5 cm^2 pieces. Before electroplating, the substrates were sequentially cleaned by 50 wt% citric acid for 15 s, deionized (DI) water, acetone, and isopropanol to remove native oxides and organic contaminants, followed by N_2 drying.

We synthesized NC-Cu and NC-Cu-Ni films (approximately 2.5 μm thick) using direct current co-electrodeposition. The base electrolyte consisted of 0.64 M $CuSO_4$ and commercial additives. To achieve varying degrees of Ni doping, we introduced different concentrations of $NiSO_4$ (0.25 M, 0.375 M, and 0.5 M) into the bath. Electroplating was conducted using a high-purity Cu anode at a constant current density of 1 A/dm^2 for 15 min, with magnetic stirring maintained at 1000 rpm to ensure uniform deposition.

To achieve the stringent surface flatness required for bonding, we planarized the electroplated films using chemical mechanical polishing (CMP; PM5, Logitech Ltd.). We applied a silica-based slurry under a polishing pressure of 4.5 psi and a slurry flow rate of 120 ml/min for 2 min. This process removed approximately 0.5 μm of the surface Cu. Post-CMP cleaning involved ultrasonic agitation in a mixture of tetraethylammonium hydroxide (TEAH) and H_2O_2 for 5 min, followed by an additional 1 min ultrasonic clean in 2 wt% citric acid to thoroughly remove residual nanoparticles.

- **Cu-Cu Bonding**

Cu-Cu thermo-compression bonding was conducted using a vacuum wafer bonder (WB-L3000, MATTECH) to prevent interfacial oxidation during heating. Before bonding, the planarized samples underwent surface activation: immersion in 2 wt% citric acid for 1 min to remove native oxides, sequential rinsing with DI water, acetone, and isopropanol, and final drying with N_2. The cleaned substrates were then diced into 1 × 1 cm² (bottom) and 0.8 × 0.8 cm² (top) chips. During assembly, the smaller top chip was precisely centered on the bottom chip. This dimensional disparity was designed to ensure a constant and well-defined contact area (0.64 cm²), thereby guaranteeing the accuracy of the applied compressive stress. Thermo-compression bonding was performed under a constant pressure of 22 MPa for 1 hour, with the bonding temperature systematically varied to investigate the low-temperature bonding performance of the symmetric and asymmetric Ni-doped Cu configurations.

- **Microstructural Characterization**

EBSD was integrated with a scanning electron microscope (SEM; Gemini 300, Carl Zeiss) to average the grain size of the microstructures. To accurately quantify the trace Ni concentrations in the doped Cu films, ICP-MS (iCAP TQ, Thermo Fisher Scientific) was employed.

To evaluate post-CMP surface cleanliness and quantify surface roughness for each sample group, we characterized surface morphology using atomic force microscopy (AFM; Dimension 3100, VEECO).

The sheet resistance of the films was measured using a four-point probe system (Loresta-GX MCP-T700, Nittoseiko Analytech). To obtain the absolute resistivity (ρ),

the actual film thickness (t) was precisely determined via focused ion beam (FIB) cross-sectional observations, and the resistivity was calculated using the equation:

$$\rho = R_s \times t$$

To directly assess electrical performance and compare with semiconductor packaging standards, we converted the measured resistivity to the International Annealed Copper Standard (IACS) conductivity percentage. The calculation is defined as the ratio of the standard resistivity of pure annealed copper at 20 °C (1.7241 μΩ·cm) to the measured resistivity of the sample, expressed as:

$$\text{IACS (\%)} = \frac{1.7241}{\rho} \times 100\%$$

- **Thermal Stability and Self-Annealing Assessment**

To evaluate the thermal stability and microstructural evolution of the NC-Cu and NC-Cu-Ni films, two primary experimental protocols were implemented: elevated-temperature vacuum annealing and long-term room-temperature self-annealing.

For thermal stability tests, the as-prepared samples were placed in a vacuum tube furnace and annealed at different temperatures for 1 h, then cooled to room temperature within the vacuum chamber. For the self-annealing assessment, as-prepared samples were stored at room temperature for 30 days to monitor microstructural changes over time. With these treatments, the grain-size distribution and electrical resistivity of the samples were recharacterized by EBSD and four-point probe measurements, respectively.

- **Bonding Quality Evaluation**

To evaluate the interfacial integrity and mechanical robustness of the Cu-Cu bonds, both microstructural characterizations and shear tests were performed.

The microstructural evolution and interfacial physical qualities were characterized using a FIB (Crossbeam 350, ZEISS) system. To prevent ion-induced recrystallization and thermal damage during milling, we deposited a protective platinum layer over the region of interest before cross-sectioning. To quantitatively evaluate microstructural evolution, we calculated the interfacial zig-zag ratio. This ratio is defined as the actual contour length of the tortuous cross-interface grain boundaries divided by the projected straight-line length of the original flat interface. We measured the contour lengths precisely from the cross-sectional FIB images using image analysis software.

We subsequently characterized the nanoscale interface using transmission electron microscopy (TEM, Thermo Fisher Scientific Helios 5). High-resolution TEM (HRTEM) and selected-area electron diffraction (SAD) were employed to analyze crystallographic orientation and verify the continuous trans-interface grain growth. Concurrently, energy-dispersive X-ray spectroscopy (EDS) was conducted to confirm the absence of residual oxides at the metallurgical joint. To quantitatively evaluate the actual bonding area, we additionally prepared plan-view TEM specimens to capture the two-dimensional spatial distribution and areal fraction of the residual voids directly across the bonding interface.

Furthermore, the mechanical strength of the bonded interfaces was quantitatively assessed through die shear testing using a shear tester (4000, Nordson DAGE). The measurements were conducted with a specific shear height of 10 μm and a constant

shear speed of 80 μm/s. The average shear strength (τ) was determined by dividing the maximum fracture load (P_{max}) by the effective bonding area (A), expressed as:

$$\tau = \frac{P_{max}}{A}$$

To ensure data reproducibility and statistical significance, a minimum of four specimens were tested for each experimental condition. During specimen preparation for bonding, using large-area copper films for direct bonding often requires high applied loads during shear testing. These high loads may cause failure at the underlying Ti adhesion layer or fracture within the Si substrate, making it difficult to evaluate the true strength of the Cu-Cu interface. To address this issue, the top Cu dies were pre-patterned using a selective etching process to form micro-mesa structures. By reducing the effective contact area, the applied stress during testing can be better concentrated at the joint. This structural design helps guide the fracture mainly along the Cu-Cu bonding interface, allowing a more reliable evaluation of the bonding strength.

References

[1] Y. H. Chen, C. A. Yang, C. C. Kuo, M. F. Chen, C. H. Tung, and W. C. Chiou, "Ultra High Density SoIC with Sub-micron Bond Pitch," 2020 IEEE 70th Electronic Components and Technology Conference (ECTC), pp. 576-581, 2020, doi: 10.1109/ECTC32862.2020.00096.

[2] M. Graef, "More Than Moore White Paper," in *2021 IEEE International Roadmap for Devices and Systems Outbriefs*, 2021, pp. 1–47, doi: 10.1109/IRDS54852.2021.00013.

[3] X. W. Lin, V. Moroz, X. Xu, Y. Gao, D. Rennie, P. Asenov, S. Smidstrup, D. Sherlekar, Z. Qin, T. Fang, J. Lee, M. Choi, and S. Jones, "Heterogeneous Integration Enabled by the State-of-the-Art 3DIC and CMOS Technologies: Design, Cost, and Modeling," 2021 IEEE International Electron Devices Meeting (IEDM), pp. 3.4.1-3.4.4, 2021, doi: 10.1109/IEDM19574.2021.9720707.

[4] J. K. Lee, S. Y. Park, Y. H. Kim, J. C. Lee, S. H. Lee, C. H. Lee, Y. T. Kwon, C. W. Lee, J. H. Kim, N. C. Kim, and Y. H. Sung, "Three-Dimensional Integrated Circuit (3D-IC) Package Using Fan-Out Technology," 2019 IEEE 69th Electronic Components and Technology Conference (ECTC), pp. 35-40, 2019, doi: 10.1109/ECTC.2019.00013.

[5] K. Oi, S. Otake, N. Shimizu, S. Watanabe, Y. Kunimoto, T. Kurihara, T. Koyama, M. Tanaka, L. Aryasomayajula, and Z. Kutlu, "Development of new 2.5D package with novel integrated organic interposer substrate with ultra-fine wiring and high density bumps," 2014 IEEE 64th Electronic Components and Technology Conference (ECTC), pp. 348-353, 2014, doi: 10.1109/ECTC.2014.6897310.

[6] C. B. Sia, "Characterization of Micro-Bumps for 3DIC Wafer Acceptance Tests," in *2019 IEEE 32nd International Conference on Microelectronic Test Structures (ICMTS)*, 2019, pp. 180–183, doi: 10.1109/ICMTS.2019.8730921.

[7] C. Chen, D. Yu, and K.-N. Chen, "Vertical interconnects of microbumps in 3D integration," *MRS Bulletin,* vol. 40, no. 3, pp. 257–263, 2015, doi: 10.1557/mrs.2015.29.

[8] Y. C. Liang, C. Chen, and K. N. Tu, "Side Wall Wetting Induced Void Formation due to Small Solder Volume in Microbumps of Ni/SnAg/Ni upon Reflow," *ECS Solid State Letters,* vol. 1, no. 4, p. P60, 2012, doi: 10.1149/2.002204ssl.

[9] Z. Chen, J. Zhang, S. Wang, and C.-P. Wong, "Challenges and prospects for

advanced packaging," *Fundamental Research,* vol. 4, no. 6, pp. 1455–1458, 2024, doi: https://doi.org/10.1016/j.fmre.2023.04.014.

[10] K. -C. Shie, P. -N. Hsu, Y. -J. Li, K. N. Tu, B. T. -H. Lin, C. -C. Chang, C. Chen, "Electromigration and Temperature Cycling Tests of Cu-Cu Joints Fabricated by Instant Copper Direct Bonding," in 2021 IEEE 71st Electronic Components and Technology Conference (ECTC), 2021, pp. 995–1000, doi: 10.1109/ECTC32696.2021.00163.

[11] K.-C. Shie, P.-N. Hsu, Y.-J. Li, K. N. Tu, and C. Chen, "Effect of Bonding Strength on Electromigration Failure in Cu–Cu Bumps," *Materials,* vol. 14, no. 21, p. 6394, 2021. [Online]. Available: https://www.mdpi.com/1996-1944/14/21/6394.

[12] S. Lhostis, B. Ayoub, H. Frémont, S. Moreau, J.-G. Mattei, P. Lamontagne, and A. Tournier, "Reliability of the hybrid bonding level using submicrometric bonding pads," Microelectronics Reliability, vol. 150, p. 115189, 2023, doi: 10.1016/j.microrel.2023.115189.

[13] K. N. Tu, C. Chen, and H.-M. Chen, *Electronic Packaging Science and Technology*. 2021.

[14] I. Panchenko, L. Wambera, M. Mueller, C. Rudolph, A. Hanisch, I. Bartusseck, and M. J. Wolf, "Grain Structure Analysis of Cu/SiO2 Hybrid Bond Interconnects after Reliability Testing," 2020 IEEE 8th Electronics System-Integration Technology Conference (ESTC), pp. 1-7, 2020, doi: 10.1109/ESTC48849.2020.9229743.

[15] E.-J. Jang, J.-W. Kim, B. Kim, T. Matthias, and Y.-B. Park, "Annealing temperature effect on the Cu-Cu bonding energy for 3D-IC integration," *Metals and Materials International,* vol. 17, no. 1, pp. 105–109, 2011, doi: 10.1007/s12540-011-0214-0.

[16] T. H. Kim, M. M. R. Howlader, T. Itoh, and T. Suga, "Room temperature Cu–Cu direct bonding using surface activated bonding method," *Journal of Vacuum Science & Technology A,* vol. 21, no. 2, pp. 449–453, 2003, doi: 10.1116/1.1537716.

[17] A. Shigetou, T. Itoh, M. Matsuo, N. Hayasaka, K. Okumura, and T. Suga, "Bumpless interconnect through ultrafine Cu electrodes by means of surface-activated bonding (SAB) method," *IEEE Transactions on Advanced Packaging,* vol. 29, no. 2, pp. 218–226, 2006, doi: 10.1109/TADVP.2006.873138.

[18] A. Shigetou, T. Itoh, and T. Suga, "Direct bonding of CMP-Cu films by

surface activated bonding (SAB) method," *Journal of Materials Science,* vol. 40, no. 12, pp. 3149–3154, 2005, doi: 10.1007/s10853-005-2677-1.

[19] D. Liu, P. C. Chen, Y. C. Tsai, and K. N. Chen, "Low Temperature Cu to Cu Direct Bonding below 150 °C with Au Passivation Layer," in *2019 International 3D Systems Integration Conference (3DIC)*, 2019, pp. 1–4, doi: 10.1109/3DIC48104.2019.9058873.

[20] H. J. Jeon and S. J. Hong, "Ammonia Plasma Surface Treatment for Enhanced Cu–Cu Bonding Reliability for Advanced Packaging Interconnection," *Coatings,* vol. 14, no. 11, p. 1449, 2024. [Online]. Available: https://www.mdpi.com/2079-6412/14/11/1449.

[21] M. P. Hsu, C. H. Chen, Z. J. Hong, T. Y. Lin, Y. C. Hung, and K. N. Chen, "Enhancement of Low-Temperature Cu-Cu Bonding by Metal Alloy Passivation in Ambient Atmosphere," *IEEE Electron Device Letters,* vol. 45, no. 8, pp. 1500–1503, 2024, doi: 10.1109/LED.2024.3416180.

[22] Z.-J. Hong, D. Liu, S.-T. Hsieh, H.-W. Hu, M.-W. Weng, C.-I. Cho, J.-H. Liu, and K.-N. Chen, "Room Temperature Cu-Cu Direct Bonding Using Wetting/Passivation Scheme for 3D Integration and Packaging," 2022 IEEE Symposium on VLSI Technology and Circuits (VLSI Technology and Circuits), pp. 387-388, 2022, doi: 10.1109/VLSITechnologyandCir46769.2022.9830175.

[23] J.-Y. Huang, D.-P. Tran, K.-P. Lee, Y.-Q. Lin, E. Kuo, T.-C. Chen, Y.-T. Chen, S. Chung, and C. Chen, "Fabrication and properties of high thermal stability nanocrystalline Cu for low temperature Cu–Cu bonding," Journal of Materials Research and Technology, vol. 35, pp. 7120–7129, 2025, doi: 10.1016/j.jmrt.2025.03.072.

[24] B. Rebhan and K. Hingerl, "Physical mechanisms of copper-copper wafer bonding," *Journal of Applied Physics,* vol. 118, no. 13, 2015, doi: 10.1063/1.4932146.

[25] M. A. Meyers, A. Mishra, and D. J. Benson, "Mechanical properties of nanocrystalline materials," *Progress in Materials Science,* vol. 51, no. 4, pp. 427–556, 2006, doi: https://doi.org/10.1016/j.pmatsci.2005.08.003.

[26] H.-E. Lin, D.-P. Tran, W.-L. Chiu, H.-H. Chang, and C. Chen, "In-situ measurement of thermal expansion in Cu/SiO2 hybrid structures using atomic force microscopy at elevated temperatures," *Applied Surface Science,* vol. 662, p. 160103, 2024, doi: https://doi.org/10.1016/j.apsusc.2024.160103.

[27] H.-E. Lin, D.-P. Tran, W.-L. Chiu, H.-H. Chang, and C. Chen, "Enhanced

thermal expansion with nanocrystalline Cu in SiO2 vias for hybrid bonding," *Applied Surface Science,* vol. 672, p. 160784, 2024, doi: https://doi.org/10.1016/j.apsusc.2024.160784.

[28] R. Huang, W. Robl, H. Ceric, T. Detzel, and G. Dehm, "Stress, Sheet Resistance, and Microstructure Evolution of Electroplated Cu Films During Self-Annealing," *IEEE Transactions on Device and Materials Reliability,* vol. 10, no. 1, pp. 47–54, 2010, doi: 10.1109/TDMR.2009.2032768.

[29] C. C. Koch, "Structural nanocrystalline materials: an overview," *Journal of Materials Science,* vol. 42, no. 5, pp. 1403–1414, 2007, doi: 10.1007/s10853-006-0609-3.

[30] C. He, J. Zhou, R. Zhou, C. Chen, S. Jing, K. Mu, Y.-T. Huang, C.-C. Chung, S.-J. Cherng, Y. Lu, K.-N. Tu, and S.-P. Feng, "Nanocrystalline copper for direct copper-to-copper bonding with improved cross-interface formation at low thermal budget," Nature Communications, vol. 15, p. 7095, 2024, doi: 10.1038/s41467-024-51510-7.

[31] K.-C. Shie, A. M. Gusak, K. N. Tu, and C. Chen, "A kinetic model of copper-to-copper direct bonding under thermal compression," *Journal of Materials Research and Technology,* vol. 15, pp. 2332–2344, 2021, doi: https://doi.org/10.1016/j.jmrt.2021.09.071.

[32] O. Anderoglu, A. Misra, H. Wang, and X. Zhang, "Thermal stability of sputtered Cu films with nanoscale growth twins," *Journal of Applied Physics,* vol. 103, no. 9, 2008, doi: 10.1063/1.2913322.

[33] O. Anderoglu, A. Misra, F. Ronning, H. Wang, and X. Zhang, "Significant enhancement of the strength-to-resistivity ratio by nanotwins in epitaxial Cu films," *Journal of Applied Physics,* vol. 106, no. 2, 2009, doi: 10.1063/1.3176483.

[34] J.-S. Chang, J.-M. Song, and C.-M. Chen, "Unidirectional cross-interface grain growth in Cu–Cu direct bonding," *Journal of Materials Research and Technology,* vol. 38, pp. 2212–2219, 2025, doi: https://doi.org/10.1016/j.jmrt.2025.08.073.